

---

This is an electronic reprint of the original article.  
This reprint may differ from the original in pagination and typographic detail.

Koskinen, Tomi; Volin, Ulrika; Tossi, Camilla; Raju, Ramesh; Tittonen, Ilkka  
**Atomic layer deposition of Zr-sandwiched ZnO thin films for transparent thermoelectrics**

*Published in:*  
Nanotechnology

*DOI:*  
[10.1088/1361-6528/ac9980](https://doi.org/10.1088/1361-6528/ac9980)

Published: 15/01/2023

*Document Version*  
Publisher's PDF, also known as Version of record

*Published under the following license:*  
CC BY

*Please cite the original version:*  
Koskinen, T., Volin, U., Tossi, C., Raju, R., & Tittonen, I. (2023). Atomic layer deposition of Zr-sandwiched ZnO thin films for transparent thermoelectrics. *Nanotechnology*, 34(3), Article 035401. <https://doi.org/10.1088/1361-6528/ac9980>

---

This material is protected by copyright and other intellectual property rights, and duplication or sale of all or part of any of the repository collections is not permitted, except that material may be duplicated by you for your research use or educational purposes in electronic or print form. You must obtain permission for any other use. Electronic or print copies may not be offered, whether for sale or otherwise to anyone who is not an authorised user.

PAPER • OPEN ACCESS

## Atomic layer deposition of Zr-sandwiched ZnO thin films for transparent thermoelectrics

To cite this article: Tomi Koskinen *et al* 2023 *Nanotechnology* **34** 035401

View the [article online](#) for updates and enhancements.

You may also like

- [\(Invited\) Effective Strategies to Improve Powerfactor of Flexible Thermoelectric Composites](#)  
Jaeyun Moon
- [P-Ca<sub>2</sub>Co<sub>2</sub>O<sub>6</sub>/n-Zn<sub>0.99</sub>Al<sub>0.01</sub>O module for high temperature thermoelectric generator](#)  
Panida Pitasuta, Supasit Paengson, Kunchit Singsoog et al.
- [\(Invited\) High Performance and Flexible Nanostructured Thermoelectric Devices By Additive Printing of Colloidal Nanocrystals](#)  
Yanliang Zhang



**IOP | ebooks™**

Bringing together innovative digital publishing with leading authors from the global scientific community.

Start exploring the collection—download the first chapter of every title for free.

# Atomic layer deposition of Zr-sandwiched ZnO thin films for transparent thermoelectrics

Tomi Koskinen<sup>1,\*</sup> , Ulrika Volin<sup>1</sup>, Camilla Tossi<sup>1,2</sup> , Ramesh Raju<sup>1</sup>  and Ilkka Tittonen<sup>1</sup> 

<sup>1</sup>Department of Electronics and Nanoengineering, Aalto University, PO Box FI-13500, Finland

<sup>2</sup>Current address: Center for Nanotechnology Innovation @ NEST, Istituto Italiano di Tecnologia, Piazza San Silvestro 12, I-56127, Pisa, Italy

E-mail: [tomi.koskinen@aalto.fi](mailto:tomi.koskinen@aalto.fi)

Received 13 May 2022, revised 1 September 2022

Accepted for publication 12 October 2022

Published 4 November 2022



CrossMark

## Abstract

Atomic layer deposited (ALD) transparent thermoelectric materials enable the introduction of energy harvesting and sensing devices onto surfaces of various shapes and sizes in imperceptible manner. Amongst these materials, ZnO has shown promising results in terms of both thermoelectric and optical characteristics. The thermoelectric performance of ZnO can be further optimized by introducing extrinsic doping, to the realization of which ALD provides excellent control. Here, we explore the effects of sandwiching of ZrO<sub>2</sub> layers with ZnO on glass substrates. The room-temperature thermoelectric power factor is maximised at 116 μW m<sup>-1</sup> K<sup>-2</sup> with samples containing a 2% nominal percentage of ZrO<sub>2</sub>. The addition of ZrO<sub>2</sub> layers is further shown to reduce the thermal conductivity, resulting in a 20.2% decrease from the undoped ZnO at 2% doping. Our results contribute to increasing the understanding of the effects of Zr inclusion in structural properties and growth of ALD ZnO, as well as the thermal and thermoelectric properties of Zr-doped ZnO films in general.

Supplementary material for this article is available [online](#)

Keywords: thermoelectric, transparent, zinc oxide, atomic layer deposition, zirconium

(Some figures may appear in colour only in the online journal)

## 1. Introduction

Thermoelectric energy conversion attracts significant interest in the sustainable energy research community thanks to its capacity of converting heat into electricity cleanly, silently, and reliably without any moving parts. Despite of the advantages over currently used commercial technologies, its large-scale deployment is still hindered by inadequate

conversion efficiency-to-cost ratio, as well as low Earth-abundance and toxicity of the best-performing materials. These drawbacks have prompted a search for sustainable thermoelectric materials and application domains in which the conversion efficiency is not the decisive figure of merit. One such domain deals with transparent thermoelectrics materials, which have a broad range of potential applications, such as sensing in smart windows and screens [1, 2], power harvesting and/or cooling in optoelectronic devices such as hybrid solar cells and consumer electronics [3]. Among the relevant material candidates, zinc oxide (ZnO) shows major benefits: it is non-toxic and highly transparent, the constituting compounds are Earth-abundant and at the same time, the manufacturing processes remain inexpensive [4]. Consequently, ZnO has been receiving wide interest as an

\* Author to whom any correspondence should be addressed.

 Original content from this work may be used under the terms of the [Creative Commons Attribution 4.0 licence](#). Any further distribution of this work must maintain attribution to the author(s) and the title of the work, journal citation and DOI.

alternative transparent conductive oxide (TCO) to indium tin oxide which, albeit more electrically conductive, presents a higher financial and environmental cost. ZnO-based TCOs are being considered in a variety of optoelectronics applications including photovoltaics [5], LEDs and flat-panel displays [6], leading to several available fabrication routes.

Obtaining the maximum thermoelectric efficiency from ZnO requires careful optimization of charge carrier concentration, which is typically accomplished by controlled introduction of external doping agents. Commonly utilized dopants include group III elements aluminium (Al), gallium (Ga) and indium (In), the doping properties of which have been studied extensively in the existing literature [7–10]. Doping with the most studied group III element, Al, however suffers from certain drawbacks: the doping efficiency remains rather low [11, 12] due to Al cations occupying interstitial lattice sites and at higher concentrations forming separate Al-rich phases [13], as well as large difference in ionic size with Zn that causes the lattice to distort. Moreover, the relative electronegativity between O and group III elements remains rather low, limiting the stability of the doping.

Since stability is a paramount factor from the practical applications perspective, the above hindrance has resulted in a search for alternatives amongst elements with larger relative electronegativity to O than Al and other group III elements. This is encountered in subgroup IV elements titanium (Ti), zirconium (Zr) and hafnium (Hf), which display weaker ionic character and in the case of Zr and Hf, ionic radii closely matching to that of Zn. While thermoelectric properties of both Ti- and Hf-doped ZnO have been reported previously [14–17], the literature still lacks results for the thermoelectric performance ensuing from Zr-doping, even though Zr has been considered a potential dopant for ZnO in related application areas during recent years [18–25]. Zr possesses several characteristics making it an attractive choice for doping ZnO: existing literature suggests that the preferred mechanism upon Zr introduction is substitution at the Zn site, in which case  $Zr^{4+}$  ion replaces a  $Zn^{2+}$  ion and acts as an effective double donor donating two electrons to the host system, therefore in theory enhancing the doping efficiency compared to, for example, Al [23, 26, 27]. On the other hand, the ionic size of  $Zr^{4+}$  matches that of  $Zn^{2+}$  closely [26], which should decrease the amount of distortion forming in the lattice upon substitutional doping.

Most of the previous studies investigating the characteristics of Zr-doped ZnO employ deposition methods which offer restricted control over the material parameters resulting from the process. An alternative deposition method that offers such control is atomic layer deposition (ALD). The use of ALD in investigating doping effects is merited by its self-limiting nature and consequently by the high level of process parameter control and accuracy, good film uniformity as well as the possibility of using low processing temperatures [28, 29]. The method has been previously utilized widely also in studying the effect of various dopants on the properties of ZnO [30]. ALD has further advantages from the industrial perspective, as the recent developments of ALD equipment also enable facile and scalable fabrication, and for instance, the exploitation of roll-to-roll manufacturing [31].

Here, we investigate the thermoelectric characteristics of ALD grown Zr-doped ZnO. The Zr doping is realised by sandwiching intermediate zirconia ( $ZrO_2$ ) layers into the ZnO film with amounts corresponding to 1%–4% nominal percentage of the total number of cycles. Our results show that the sandwiched Zr acts as an n-type dopant in ZnO, with the charge carrier concentration increasing from  $2.1 \cdot 10^{19}$  to  $3.1 \cdot 10^{19} \text{ cm}^{-3}$  at 1% doping while staying approximately at the same level also at higher doping percentages. The increase in charge carrier concentration results in increased electrical conductivity with the cost of decreased Seebeck coefficient value, yielding a maximum room-temperature power factor of  $116.1 \mu\text{W m}^{-1} \text{ K}^{-2}$  at nominal doping percentage of 2%. As the characteristics of ALD-grown ZnO have been shown to alter upon subjection to elevated temperatures [14, 32], we also record the change in the thermoelectric properties at different phases of a heating cycle to quantify the effect at different doping concentrations. Temperature-dependent thermoelectric characterization shows that the film properties are altered upon annealing to 180 °C and subsequent cooling, with all films showing a decrease in electrical conductivity with a simultaneous increase in the absolute Seebeck coefficient, resulting in an overall detrimental effect to the power factor. The magnitude of the temperature-induced change is mitigated at increasing doping percentages which suggests that increasing Zr incorporation increases the thermal stability in ALD-grown ZnO.

## 2. Experimental methods

### 2.1. Atomic layer deposition

ZnO and Zr-doped ZnO (ZZO) were grown on pre-cleaned borosilicate glass and silicon in a Beneq TFS-500 ALD reactor at a temperature of 150 °C. Diethylzinc (DEZn) and  $H_2O$  were used as precursors for ZnO, while tetrakis-ethylmethylaminozirconium (TEMAZ) and  $H_2O$  were used for the  $ZrO_2$  doping layers. The solid TEMAZ source was kept at a temperature of 50 °C. The deposition was carried out at a reactor pressure of  $\sim 0.65$  mbar with  $N_2$  as the carrier gas. The precursor pulsing cycle for ZnO consisted of three 200 ms DEZn and three 200 ms  $H_2O$  pulses with 4.5 s purge after each precursor. Similarly, for  $ZrO_2$  the cycle consisted of 250 ms  $H_2O$  and 1 s TEMAZ pulses with 6 s purge after each precursor pulse. To fabricate sandwiched films, the ZnO and  $ZrO_2$  cycles were combined into supercycles consisting of  $200-200n+5$  ZnO and  $200n$   $ZrO_2$  cycles, in which  $n$  covered a range from 0 to 0.04 in order to deposit samples with nominal doping percentages of 0%–4%. In total three consecutive supercycles were deposited for each sample, resulting in superstacks.

### 2.2. Structural characterization

The thicknesses of the films resulting from the ALD process were analysed with a Semilab SE-2000 spectroscopic ellipsometer in the mapping mode averaging over five positions over the sample area. Sample surfaces were further

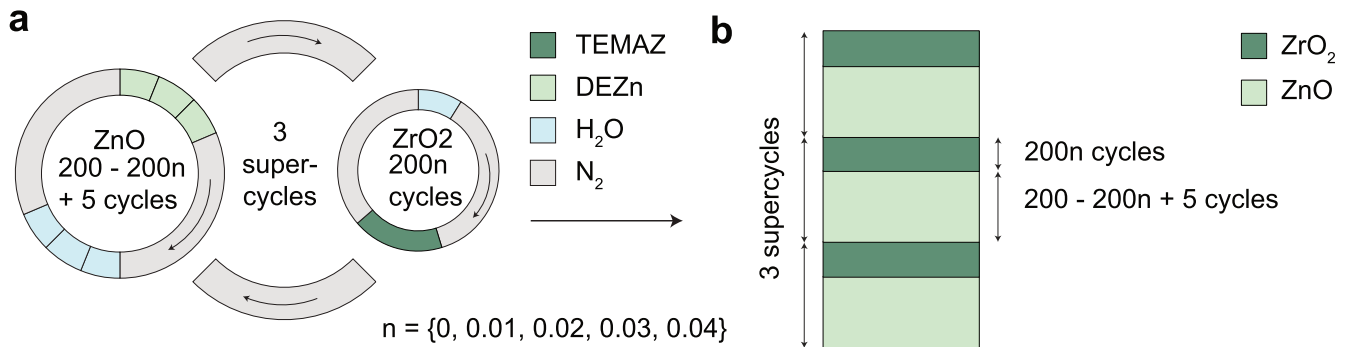


**Figure 1.** (a) ALD cycle parameters for both ZnO and ZrO<sub>2</sub>. (b) the resulting superstack structure.

characterized with scanning electron microscopy (SEM, Zeiss Supra 40) and atomic force microscopy (AFM, Bruker Dimension Icon). The transmission spectra were acquired in the visible range under normal incidence using a halogen light source (Ocean Optics HL-2000-FHSA). The transmitted radiation was collected with an integrating sphere and fed to a grating spectrometer (Ocean Optics).

Crystal structure was observed by grazing incidence x-ray diffraction (GIXRD, Rigaku SmartLab XRD, Cu K<sub>α,β</sub>). Thinned cross-section lamellae were cut from the ZnO films deposited on silicon substrates with a focused ion beam microscope (JEOL JIB-4700F). An analytical high-resolution transmission electron microscope (HR-TEM) with an acceleration voltage of 200 kV (JEOL JEM-2800) was used for confirming the crystal structure by HR-TEM and by selected area diffraction (SAD), while high-speed energy-dispersive x-ray spectroscopy (EDX) was used to map the elemental composition of the lamellae.

### 2.3. Electrical and thermoelectric characterization

The samples were prepared for characterization by dicing the glass into 4 mm × 20 mm or 12 mm × 12 mm chips and by depositing Ti/Au (20 nm/40 nm) electrical contact pads using e-beam evaporation (Edwards E306A). Electrical conductivity and Seebeck coefficient were measured from room temperature to 180 °C and back under He atmosphere in a Linseis LSR-3 setup with five temperature gradients with 10 min stabilization time for each gradient imposed in each temperature. Room-temperature charge carrier concentration and mobility were obtained using an Ecopia HMS-5300 hall measurement system and the van der Pauw geometry.

### 2.4. Thermal characterization

The thermal properties of the samples were investigated using a nanosecond transient thermoreflectance setup (Linseis TF-LFA). The setup is an optical pump-probe system using a 1064 nm Q-switched pump laser for heating a spot on the sample surface and a 476 nm diode laser for probing the resulting temperature transient. The samples were prepared for the measurement by depositing a Ti/Au (nominal 20 nm/200 nm) transducer layer using e-beam evaporation. Transducer thickness was confirmed using a stylus profilometer (Bruker Dektak XT). The measurement was

conducted in room temperature and averaged over 80 pump laser shots in six spots for each sample to obtain a spatial average.

## 3. Results and discussion

### 3.1. Growth results and structural properties

The Zr-doped ZnO samples are grown using a combination of ZnO and ZrO<sub>2</sub> ALD-cycles, as illustrated in figure 1(a) and outlined in the previous section. Instead of distributing the ZrO<sub>2</sub> cycles evenly, the chosen fabrication scheme results in the sandwich-type structure exhibiting a clustered dopant allocation presented in figure 1(b). The approach is chosen to minimize the disruption to ZnO nucleation after dopant cycle introduction, while simultaneously attempting to achieve a high enough doping level [8, 14]. The ALD process produces films of high optical transparency as presented in figure 2(a). The transmission spectra for each sample are presented in figure S4, supporting information, with no relevant observable changes between samples.

The films display a decreasing thickness trend as a function of increasing number of ZrO<sub>2</sub> cycles, as observed in spectroscopic ellipsometry and presented in table 1. This trend is explained by the growth rates of the respective growth cycles; the ZnO process displays a growth-per-cycle of approximately 2.1 Å/cycle as calculated from the reference sample, whereas the growth rate for ZrO<sub>2</sub> is lower at 1.37 Å/cycle as calculated from a separate process validation sample with 400 cycles of ZrO<sub>2</sub>.

SEM investigation of the film surfaces presented in figures 2(c) and figure S1 show a clear difference in grain size and distribution between ZnO and the Zr-doped samples. Further characterization with an atomic force microscope (AFM) shows that the surface roughness of the films decreases as a function of increasing Zr content in the sandwiched samples, as presented in figures 2(d) and figure S1(b), supporting information. Quantitative analysis of the RMS roughness is included in table 1, showing a clear decreasing trend as a function of increasing Zr doping.

Additional insight into the structural properties is gained via grazing incidence x-ray diffraction (GIXRD) measurements. Figure 2(b) presents the patterns for each sample, showing peaks

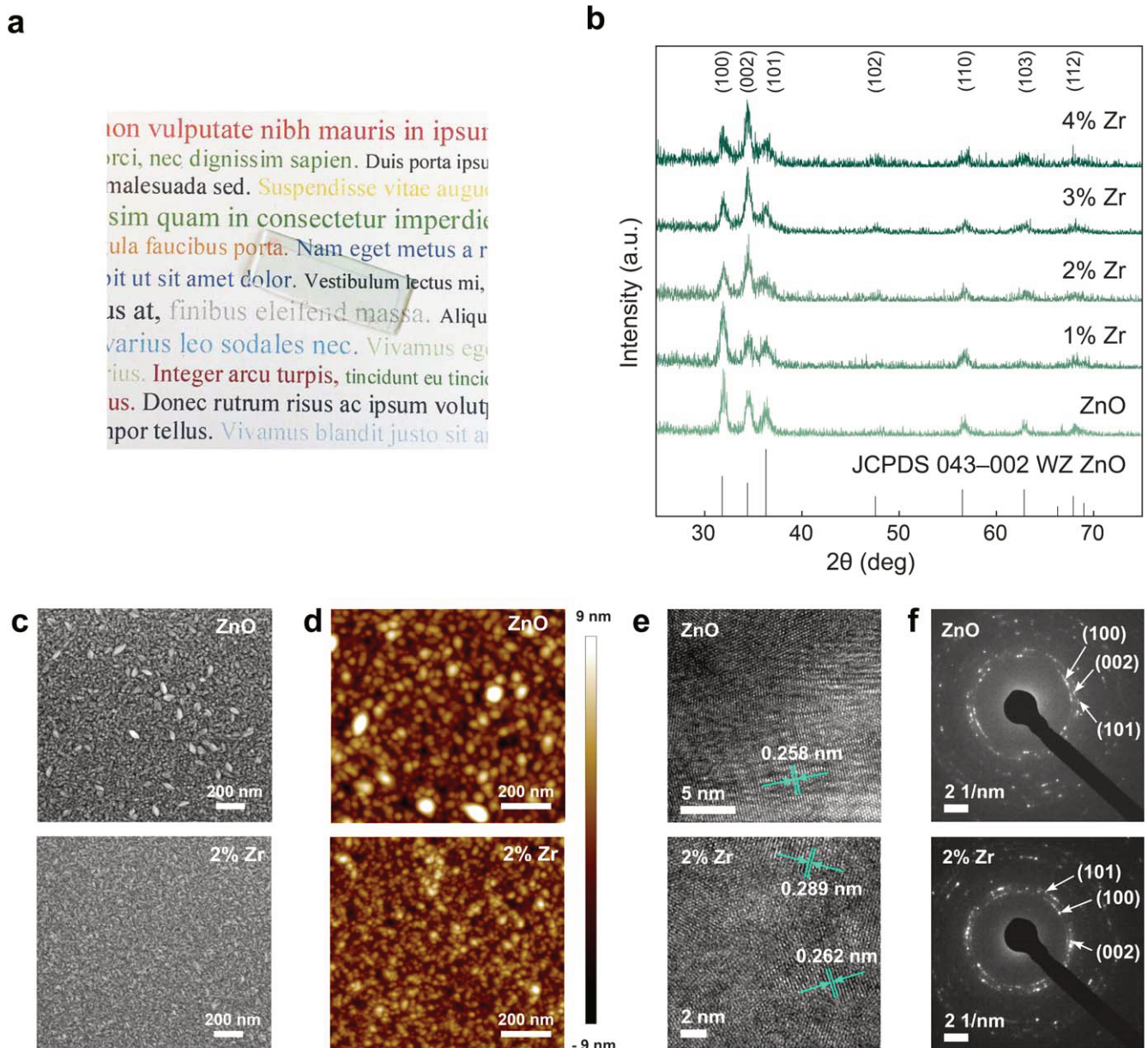


**Figure 2.** (a) Photograph of 2% Zr-ZnO film on glass. (b) GIXRD spectra for the films along with a standard diffraction pattern. (c) SEM micrographs of the ZnO reference and 2% Zr-ZnO film surfaces. (d) AFM micrographs of the ZnO reference and 2% Zr-ZnO film surfaces. (e) TEM micrographs of cross-sections of the reference ZnO film and of 2% Zr-ZnO film. (f) SAD patterns of cross-sections of the reference ZnO film and of 2% Zr-ZnO film.

**Table 1.** Sample thicknesses and uniformities based on spectroscopic ellipsometry.

Sample	Thickness (nm)	Uniformity (%)	RMS roughness (nm)
ZnO	131.03	0.9837	2.62
1%	126.20	1.3115	2.39
2%	127.41	0.7571	2.00
3%	127.88	1.2547	1.32
4%	125.28	0.5868	1.21

characteristic to wurtzite (WZ) ZnO as further confirmed by the close match to JCPDS 043-002 standard diffraction pattern for bulk WZ ZnO. The close resemblance indicates that the inclusion of Zr cycles has not resulted in major ZrO<sub>2</sub> formation [24],

as the corresponding peaks in the XRD spectra are completely absent. The peaks obtained from undoped ZnO correspond to nonpolar (100) and (101) and polar (002) planes, the first two of which are characteristic to the growth temperature regime and indicative of polycrystalline mixture of grains with the *c*-axis parallel and perpendicular to the substrate surface, respectively [33]. At 0% doping the (100) peak is the strongest, which is typical for ZnO grown on glass and Si [33, 34]. When the doping percentage is increased, the relative magnitude of the (002) peak increases compared to (100) and (101) peaks, and at 2% doping the (002) peak exceeds the (100) peak. This is indicative of the preferred growth direction changing from the (100) plane to (002) plane. A qualitatively similar shift in the peak magnitudes upon increased doping percentage has previously been observed also with other dopant distribution

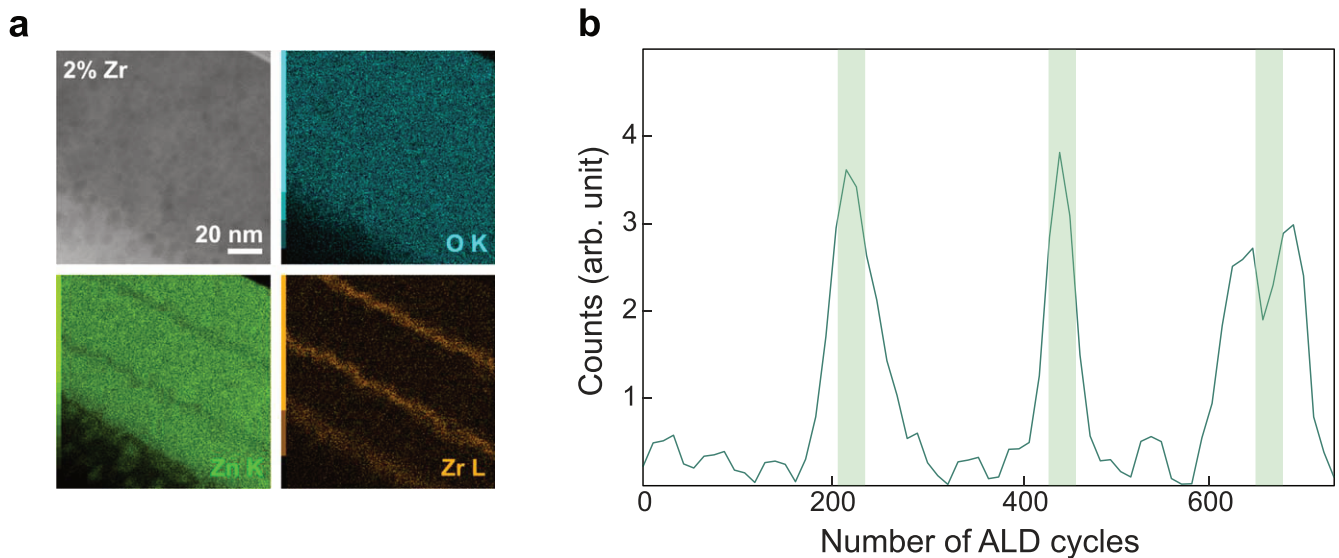


**Figure 3.** (a) Scanning-transmission electron micrograph and EDX spectroscopic imaging of the 2% Zr-ZnO cross-section cut. (b) EDX profile of Zr across the section.

schemes [25] and Zr doped ZnO deposited via alternative methods [18], as well as with Al and Hf doping in ALD grown films when a similar clustered doping scheme has been exploited [8, 14]. The reason for the said change is attributed to the substrate sensitivity of the ZnO growth [35]; the Zr saturated surface behaves differently in this regard from glass or Si. The reason for preferring the (002) orientation could originate from the polarity of the different planes: in the polar (002) plane the crystal grains have either positively or negatively charged plane exposed depending on if the termination occurs with  $\text{Zn}^{2+}$  or  $\text{O}^{2-}$  ions at the surface, respectively. The charge difference between Zr and Zn can disturb the charge neutrality of the intrinsically preferred growth direction along the (100) plane [36] which then results in favouring the growth along the (002) plane instead when ZnO growth is resumed after dopant cycle introduction. Finally, the crystallite sizes in the films are estimated using the Scherrer formula [37] from gaussian fits to (100), (101) and (102) peaks for each sample. The undoped ZnO shows an average crystallite size of 12.1 nm. Upon increasing Zr concentration, the crystallite size decreases steadily and reaches 7.8 nm at 4% doping, which is in good qualitative agreement with the result obtained for surface RMS roughness.

The cross-sections prepared by focused  $\text{Ga}^+$  ion beam milling of the ALD-grown films are examined by analytical high-resolution transmission electron microscopy, obtaining further structural analysis, as detailed in figures 2 (e)–(f), and a map of the chemical elements, as figure 3(a) shows. Corresponding maps for other doping percentages are provided in figure S2, supporting information. The distribution of Zr layers is further highlighted in the EDX profile presented in figure 3(b).

Direct observation of the cross-sections shows crystallites of 5–10 nm in size, where crystallographic planes can be detected (for example, figure 2(e) compares a ZnO sample with a 2%  $\text{ZrO}_2$  sample, highlighting the spacing between the (002) planes and the (100) planes, which agrees with the XRD result.) An accurate measurement of the plane spacing

can be inferred by the SAD patterns (figures 2(f), S1(c), (d) and S3, supporting information): the measurements show greater lattice parameters for the doped samples, which can be attributed to the larger atomic radius of Zr, but no significant trend with respect to the Zr content, implying that the presence of the dopant is enough to increase the size of the elementary crystal cell. Additionally, as the doping increases, the diffraction pattern becomes clearer and brighter, which suggests an increase in crystallinity. This is highlighted particularly in the ring given by the (002) plane, confirming the growth preference in the [002] direction.

### 3.2. Electrical and thermoelectric properties at the room temperature

The effect of the Zr doping on the electrical transport characteristics is first investigated from charge carrier concentration measurements conducted in a hall measurement system in the van der Pauw geometry. Charge carrier concentration and mobility as a function of doping percentage are presented in figures 4(a)–(b). The undoped sample shows a charge carrier concentration of  $2.1 \cdot 10^{19} \text{ cm}^{-3}$ , which is slightly higher than what has been reported previously for undoped ZnO grown at the same temperature using a similar process [8]. Introducing the Zr cycles in the ZnO host structure shows an increase to  $3.1 \cdot 10^{19} \text{ cm}^{-3}$  already at 1% nominal doping with higher doping percentages resulting in values setting in the close vicinity. Comparison to previous studies exploiting ALD on fabricating Zr-doped ZnO have found charge carrier concentrations up to  $3 \cdot 10^{20} \text{ cm}^{-3}$  at similar doping concentrations [21, 23], which in this case can be attributed to the higher growth temperatures exploited in these studies and the thus resulting differences in crystallinity [38]. Hall mobility, presented in figure 4(b), shows a modest decrease as the doping increases: the inclusion of Zr atoms, despite providing additional charge carriers also induces ionized impurity scattering. At the same time, the increase in charge carrier concentration also promotes electron–electron

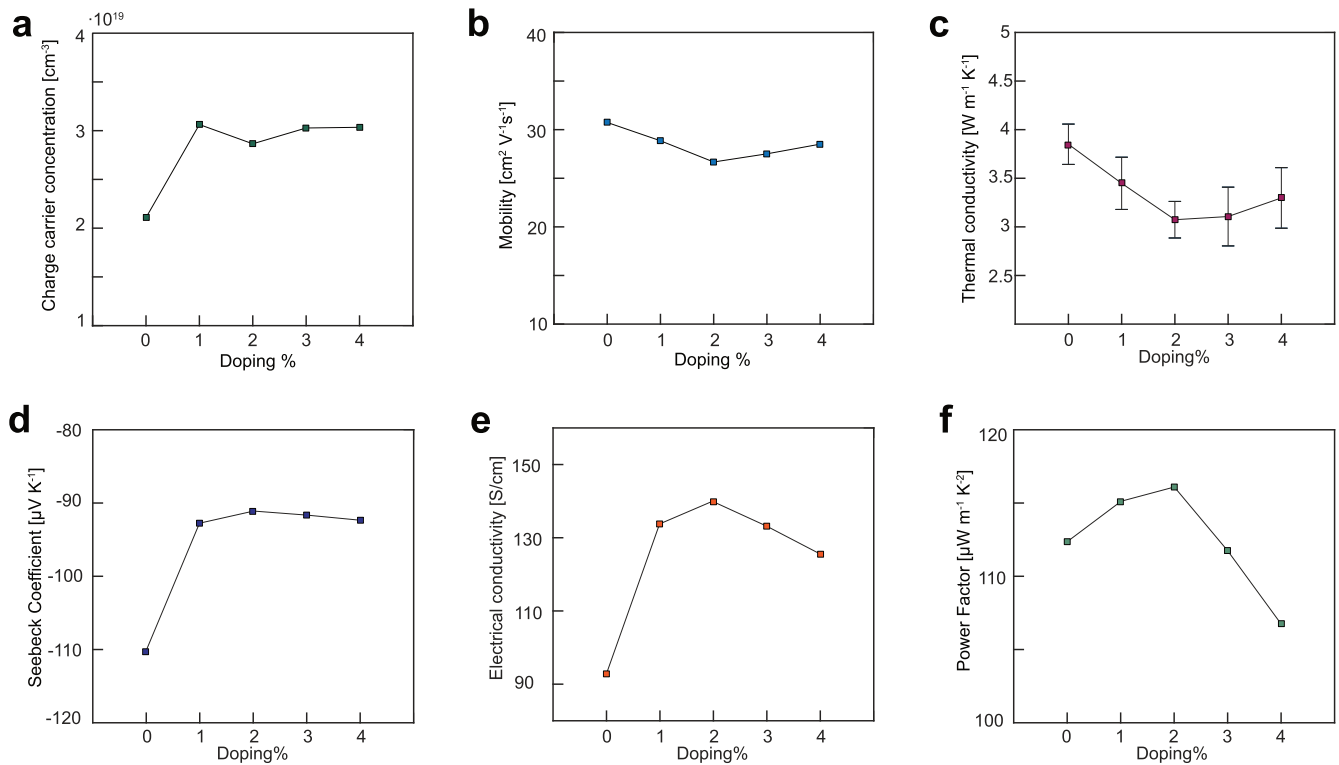


**Figure 4.** (a) Absolute value of charge carrier concentration, (b) hall mobility, (c) thermal conductivity, (d) Seebeck coefficient, (e) electrical conductivity and (f) power factor at each doping percentage in room temperature.

scattering, which together hinder the charge mobility. The change in mobility is of the same order of magnitude as previously observed for Al, Ti and Hf doping employed in the same manner. The charge carrier concentration and mobility data show a discrepancy with the electrical conductivity data obtained from the thermoelectric measurement; this is explained by the fact that the two measurements require different sample geometries and therefore highlight variation in fabrication process uniformity. The hall measurement data, nevertheless, advances that the increase in electrical conductivity is driven by a doping-induced increase in charge carrier concentration.

Interestingly, the direct dopant substitution has been proposed to occur in ZnO only with one crystal growth orientation if multiple ones are present, as presented for doping with Hf, another subgroup IV element [39]. In this case, the direct substitution was proposed to take place in domains corresponding to (100) planes, and the enhanced contribution of (002) orientation at increasing Hf concentration would essentially decrease doping efficiency, as the direct substitution would not be preferred in this orientation. The similarity between previous observations from Hf doping and the ones obtained here for Zr doping is likely explained with the closely alike ionic radii (71 pm versus 74.5 pm) [40]. On the other hand, the slight difference in the ionic radii of Zn<sup>2+</sup> and Zr<sup>4+</sup> (74 pm versus 74.5 pm) [41] could play a role by inducing tensile stress in the case of substitutional doping.

The room-temperature results for the Seebeck coefficient  $S$  and electrical conductivity  $\sigma$  for each doping percentage are presented in figure 3(b) along with the resulting thermoelectric power factor  $PF = S^2\sigma$ . As expected, the samples show decreasing  $|S|$  and increasing  $\sigma$  as a function of increasing Zr

content. The room-temperature PF is maximised for the sample with a nominal doping percentage of 2%, after which it sharply declines. This non-monotonic behaviour as a function of increasing doping is again qualitatively similar to what has been previously observed with the optoelectronic properties of Hf-doped ZnO [39] and is well aligned with the change in the dominating growth orientation observed in the GIXRD results. Mitigated substitutional Zr incorporation upon the enhancement of (002) growth direction would therefore explain the decreasing electrical conductivity at higher doping concentrations; the dopants would simply not be activated due to not reaching the right sites. A quantitative difference between our results and other studies investigating ZnO doping with subgroup IV elements lies in the magnitude of doping percentages at which the non-monotonous behaviour takes place; typically, changes in electronic and optical properties have been observed at doping percentages above 5 at% [23], while here qualitatively similar behaviour is seen already at much lower nominal doping percentages (based on the growth rates, 2% nominal doping corresponds to  $\sim 1.3$  at%). This is likely caused by the sandwiched doping scheme, due to which the local Zr concentration at the doping sites is much higher than what the nominal doping percentage suggests, and therefore at these sites the Zr inclusion also has relatively greater effect on the crystal growth and subsequent properties.

### 3.3. Thermal properties and thermoelectric figure of merit

As witnessed in structural characterization conducted in GIXRD and SEM/AFM, the introduction of ZrO<sub>2</sub> layers alters the crystalline structure of the superstack films in

comparison to the pure ZnO sample especially in terms of the preferred crystal orientation and grain size. This is expected to also affect the thermal transport properties via the mechanism of classical size effect and increased phonon scattering at grain interfaces. Room-temperature thermal conductivity results measured using nanosecond transient thermoreflectance [42] are presented in figure 4(c). The thermal conductivity shows a substantial decrease of 10.4% compared to bare ZnO already at 1% nominal doping and is minimized at 2% doping at  $\kappa = 3.07 \text{ W m}^{-1} \text{ K}^{-1}$ . At 3% and 4% doping the value slightly increases from the minimum but does not surpass the value obtained at 1%. The observed trend is qualitatively alike to what is witnessed with the charge carrier concentration data and indicates that increasing the Zr doping percentage further does not result in drastic changes in the thermoelectric transport properties in room temperature. A previous report on the thermal conductivity of Al-doped ZnO thin films [43] shows qualitatively similar behavior, with a film thickness of 150 nm and a decrease from  $5.6 \text{ W m}^{-1} \text{ K}^{-1}$  to 1.1 at 1.5% doping. We note that the value obtained for the undoped ZnO in this work is rather low, compared to values of  $\sim 40 \text{ W m}^{-1} \text{ K}^{-1}$  obtained for ALD-grown ZnO previously [44, 45], which could be explained by higher crystallinity resulting from higher growth temperatures exploited in the referred works.

Having obtained the thermoelectric power factor and the thermal conductivity in room temperature, we can now calculate the thermoelectric figure of merit  $zT = S^2 \sigma T \kappa^{-1}$  as a function of doping percentage in the room temperature. We obtain  $zT = 0.0087$  for the reference ZnO sample, and the highest  $zT = 0.011$  for the sample with 2% Zr content. Intriguingly, the 2% sample that displays the highest PF at the room temperature also possessed the lowest thermal conductivity, resulting in best performance prior to thermal treatment amongst the doped samples.

### 3.4. Temperature-dependent properties

The thermoelectric properties were further investigated as a function of temperature by ramping the temperature up to 180 °C at 30 °C intervals and subsequently bringing it back to room temperature. The corresponding Seebeck coefficient, electrical conductivity and power factor curves are presented in figure 5 for both the heating and cooling phases of the thermal cycle separately. As shown for the room-temperature properties, the doped samples have a similar Seebeck coefficient among themselves and show highly similar temperature dependent behaviour, as presented in figure 5(a). The absolute value of the Seebeck coefficient increases as a function of temperature for all samples, with the undoped ZnO showing the highest value of  $-139.6 \mu\text{V K}^{-1}$  at 180 °C.

Simultaneously, the electrical conductivity of all samples decreases with increasing temperature as shown in figure 5(b). This phenomenon has been observed to take place in ALD grown ZnO films also in previously published reports [14, 32], and it has been attributed to the forming of zinc vacancies that compensate zinc interstitial defects formed during the growth due to the insufficient oxidation capacity of

the water precursor. Notably, this effect is much larger for doped samples than the undoped reference sample, and at the temperature of 180 °C the doped samples have an electrical conductivity similar to the undoped one. As a result, the highest power factor of  $155 \mu\text{W m}^{-1} \text{ K}^{-2}$  at 180 °C is achieved with the undoped sample as presented in figure 5(c).

The behaviour during the cooling stage of the thermal cycle is presented in figures 5(d)–(f). The absolute Seebeck coefficient decreases slightly from the obtained level but does not return to the original room temperature value. At the same time, the electrical conductivity keeps decreasing and shows remarkably smaller values than at the beginning of the thermal cycle. The degradation in the electrical conductivity is greatest for the 2% sample, which rather interestingly shows the worst PF among the samples after the cycle. At the end of the cycle, all doped samples show PF smaller than the undoped ZnO, indicating that the introduction of dopants decreases the thermal stability.

Nevertheless, the changes caused by the thermal cycle are not similar in all doped samples, but instead a non-monotonous dependence on the doping percentage is observed. As noted above, the 2% sample that showed the highest performance in room temperature prior to the thermal cycle now displays the lowest performance with substantial changes both in the Seebeck coefficient and electrical conductivity. However, when the doping percentage is further increased, the change in room-temperature power factor is mitigated and at 4% doping, shows temperature-dependent behaviour resembling that of the undoped sample. The room temperature properties of each sample after the cycle have been gathered in figures 5(g)–(i).

A possible explanation for the lower thermal stability of the 1%–3% samples is hinted in the GIXRD results obtained prior to the thermal cycling; the largest change after the cycle takes place at 2%, which is also the doping percentage at which the change in the preferred growth orientation occurs. This indicates that when extrinsic Zr dopants are incorporated in the structure, the structure with the preferred (002) orientation is more stable under thermal cycling; the fact that the change in power factor as a function of doping percentage is non-monotonous implies that Zr inclusion alone does not improve the stability. Alternatively, the doping in 1%–2% samples prior to cycling could be contributed by defects that are compensated during the annealing, whereas in 3%–4% samples the doping would be caused by Zr inclusion alone. However, this somewhat contradicts with the prior discussion on differences in dopant incorporation in the (001) and (002) crystal orientations.

In the literature, annealing cycles comparable to the one conducted in this work are typically claimed to stabilize the structure, i.e. the properties resulting from the treatment are those that remain over time. We gather insight on this aspect by measuring the room-temperature characteristics from the once-annealed samples after storing them in air for ten weeks. The obtained room-temperature electrical conductivities closely match those obtained at the end of the annealing cycle, but the absolute Seebeck coefficient values are slightly lower, correspondingly resulting in lower power factor values. The

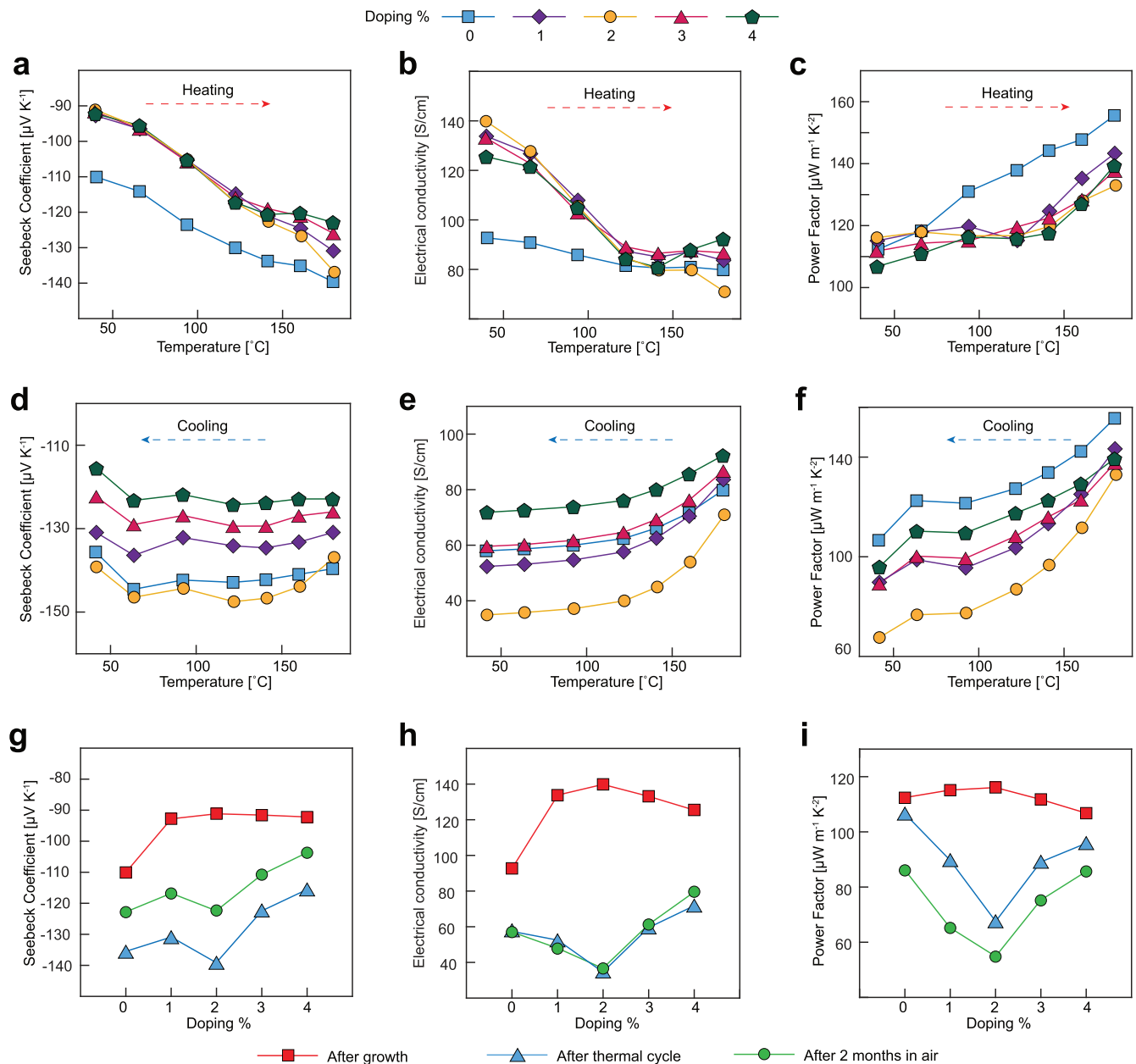


**Figure 5.** (a) Seebeck coefficient, (b) electrical conductivity and (c) power factor at each doping percentage at the heating stage of the thermal cycle. (d) Seebeck coefficient, (e) electrical conductivity and (f) power factor at each doping percentage at the cooling stage of the thermal cycle. (g) Seebeck coefficient, (h) electrical conductivity and (i) power factor at room temperature before the cycle, after the cycle and after storing for ten weeks in air.

decline is similar for all samples regardless of the doping percentage. A possible reason for the observed decline might be that the Seebeck coefficient value obtained at the end of the annealing cycle is not stable, but it further decreased when the temperature slightly decreased after the samples were removed from the measurement chamber. In this case, the observed decline would not be caused by storing and the samples would be quite stable in air, which is further supported by the unchanged electrical conductivity values during the ten-week gap in between the two measurements.

Comparison to other works on ALD-grown Zr-doped ZnO [21, 23, 24] shows that the electrical conductivity values obtained in this work are lower than in the referenced works.

This is a direct consequence of lower charge carrier concentration values obtained here ( $\sim 3 \cdot 10^{19} \text{ cm}^{-3}$ ) which are generally an order of magnitude lower than in the referenced works ( $1\text{--}5 \cdot 10^{20} \text{ cm}^{-3}$ ) and can be attributed to the lower growth temperature used in this work. On the other hand, films with higher carrier concentration likely show lower Seebeck coefficient compared to what was now obtained.

To our knowledge, previous results for the thermoelectric properties of ALD-grown Zr-doped ZnO have not been reported. Nevertheless, results for thermoelectric properties of ALD-grown ZnO doped with other subgroup IV elements (Ti and Hf) exist [14], as briefly discussed in the introduction. Comparison of the electrical characteristics shows that at the

room temperature, properties resulting from Zr-doping more closely resemble those emerging from Hf-doping instead of Ti-doping, both in terms of the Seebeck coefficient and the electrical conductivity. The similarities between XRD spectra for Zr- and Hf-doped ZnO confirm the comparison, as mentioned in the structural characterization section. The room temperature power factor values obtained for Zr-doped ZnO are close to those obtained for Ti and Hf-doped ZnO, whereas in terms of temperature stability, Zr-doping provides an intermediate performance between Ti- and Hf-doping.

#### 4. Conclusions

We have presented results for thermoelectric, thermal, and structural properties of atomic layer deposited Zr-ZnO sandwich structures grown at 150 °C. The inclusion of Zr into the ZnO structure resulted in enhanced charge carrier concentration with a value of  $3.1 \cdot 10^{19} \text{ cm}^{-3}$  at 1% doping, which led to an increase in the electrical conductivity and a decrease in the absolute Seebeck coefficient at room temperature, respectively. The highest room-temperature power factor is obtained at 2% nominal Zr content. When cycling the temperature to 180 °C and back to room temperature, the films underwent changes that led to a decrease in electrical conductivity and a simultaneous increase in the Seebeck coefficient resulting in a degraded power factor after the cycle. The magnitude of these changes is dependent on the doping concentration, with the largest changes at 2% doping level while the 4% doping level shows temperature-dependent behaviour closely corresponding to that of undoped ZnO.

#### Acknowledgments

The authors acknowledge the financial support from the Academy of Finland projects 319018 eVapor and 329406 CarbonSurf as well as from the Photonics Flagship PREIN. T. K. acknowledges the doctoral school of Aalto University School of Electrical Engineering, Walter Ahlström foundation and Waldemar Von Frenckell foundation for financial support. C.T. acknowledges the financial support of the Yrjö, Vilho ja Kalle Väisälä Fund and of the Finnish Academy of Sciences and Letters. The experimental work was carried out in Micronova, the nanofabrication facility of Aalto University. Edgar Maiorov is acknowledged for ALD equipment support. Dr Vladimir Kornienko is acknowledged for helping with the transmission measurement. The characterization by XRD, TEM and FIB was carried out in the Nanomicroscopy Center of Aalto University.

#### Data availability statement

The data that support the findings of this study are available upon reasonable request from the authors.

#### ORCID iDs

Tomi Koskinen  <https://orcid.org/0000-0001-6883-4181>  
 Camilla Tossi  <https://orcid.org/0000-0002-0450-6995>  
 Ramesh Raju  <https://orcid.org/0000-0002-1802-9077>  
 Ilkka Tittonen  <https://orcid.org/0000-0002-2985-9789>

#### References

- [1] Ruoho M, Juntunen T and Tittonen I 2016 Large-area thermoelectric high-aspect-ratio nanostructures by atomic layer deposition *Nanotechnology* **27** 355403
- [2] Jaakkola K and Tappura K 2018 Exploitation of transparent conductive oxides in the implementation of a window-integrated wireless sensor node *IEEE Sens. J.* **18** 7193–202
- [3] Wang X, Suwardi A, Lim S L, Wei F and Xu J 2020 Transparent flexible thin-film p–n junction thermoelectric module *Npj Flex. Electron.* **4** 1–9
- [4] Tappura K, Juntunen T, Jaakkola K, Ruoho M, Tittonen I, Ritala R and Pudas M 2020 Large-area implementation and critical evaluation of the material and fabrication aspects of a thin-film thermoelectric generator based on aluminum-doped zinc oxide *Renew. Energy* **147** 1292–8
- [5] Huang J, Yin Z and Zheng Q 2011 Applications of ZnO in organic and hybrid solar cells *Energy Environ. Sci.* **4** 3861–77
- [6] Belyaev V, Abduev A, Akhmedov A, Asvarov A, Skvortsov A and Plentsova D 2019 34 .2: invited paper: ZnO based transparent conductive oxides for to-date flat panel displays *SID Symp. Dig. Tech. Pap.* **50** 372–5
- [7] Lee D-J, Kim H-M, Kwon J-Y, Choi H, Kim S-H and Kim K-B 2011 Structural and electrical properties of atomic layer deposited Al-Doped ZnO films *Adv. Funct. Mater.* **21** 448–55
- [8] Ruoho M, Pale V, Erdmanis M and Tittonen I 2013 Influence of aluminium doping on thermoelectric performance of atomic layer deposited ZnO thin films *Appl. Phys. Lett.* **103** 203903
- [9] Fan P, Li Y, Zheng Z, Lin Q, Luo J, Liang G, Zhang M and Chen M 2013 Thermoelectric properties optimization of Al-doped ZnO thin films prepared by reactive sputtering Zn–Al alloy target *Appl. Surf. Sci.* **284** 145–9
- [10] Tsubota T, Ohtaki M, Eguchi K and Arai H 1997 Thermoelectric properties of Al-doped ZnO as a promising oxide material for high-temperature thermoelectric conversion *J. Mater. Chem.* **7** 85–90
- [11] Lee D-J, Kim K-J, Kim S-H, Kwon J-Y, Xu J and Kim K-B 2013 Atomic layer deposition of Ti-doped ZnO films with enhanced electron mobility *J. Mater. Chem. C* **1** 4761–9
- [12] Wu Y, Hermkens P M, van de Loo B W H, Knoops H C M, Potts S E, Verheijen M A, Roozeboom F and Kessels W M M 2013 Electrical transport and Al doping efficiency in nanoscale ZnO films prepared by atomic layer deposition *J. Appl. Phys.* **114** 024308
- [13] Gabás M *et al* 2013 Differences in n-type doping efficiency between Al- and Ga-ZnO films *J. Appl. Phys.* **113** 163709
- [14] Felizco J, Juntunen T, Uenuma M, Etula J, Tossi C, Ishikawa Y, Tittonen I and Uraoka Y 2020 Enhanced thermoelectric transport and stability in atomic layer deposited-HfO<sub>2</sub>/ZnO and TiO<sub>2</sub>/ZnO-sandwiched multilayer thin films *ACS Appl. Mater. Interfaces* **12** 49210–8
- [15] Shih B-W, Hsieh W-P, Shyue J-J and Tsai F-Y 2020 Enhanced thermoelectric properties of atomic-layer-deposited Hf: Zn<sub>160</sub>/180 superlattice films by interface-engineering *Ceram. Int.* **46** 7122–30

- [16] Park K and Ko K Y 2007 Effect of TiO<sub>2</sub> on high-temperature thermoelectric properties of ZnO *J. Alloys Compd.* **430** 200–4
- [17] Hong M-H, Choi H, Kim Y, Kim T, Cho H H, Driss Z, Driss D, Bouabidi A, Euchy S and Park H-H 2019 Ti doping effects on the seebeck coefficient and electrical conductivity of mesoporous ZnO thin film *Mater. Chem. Phys.* **235** 121757
- [18] Paul G K, Bandyopadhyay S, Sen S K and Sen S 2003 Structural, optical and electrical studies on sol–gel deposited Zr doped ZnO films *Mater. Chem. Phys.* **79** 71–5
- [19] Yadav S K, Vyas S, Chandra R, Chaudhary G P and Nath S K 2009 Study of electrical and optical properties of Zr-doped ZnO thin films prepared by DC reactive magnetron sputtering *Adv. Mater. Res.* **67** 161–6
- [20] Zhang H, Lei C, Liu H and Yuan C 2009 Low-temperature deposition of transparent conducting ZnO:Zr films on PET substrates by DC magnetron sputtering *Appl. Surf. Sci.* **255** 6054–6
- [21] Lin M-C, Chang Y-J, Chen M-J and Chu C-J 2011 Characteristics of Zr-Doped ZnO thin films grown by atomic layer deposition *J. Electrochem. Soc.* **158** D395
- [22] Gokulakrishnan V, Parthiban S, Jeganathan K and Ramamurthi K 2011 Investigation on the effect of Zr doping in ZnO thin films by spray pyrolysis *Appl. Surf. Sci.* **257** 9068–72
- [23] Herodotou S, Treharne R E, Durose K, Tatlock G J and Potter R J 2015 The effects of Zr doping on the optical, electrical and microstructural properties of thin ZnO films deposited by atomic layer deposition *Materials* **8** 7230–40
- [24] Wu J, Zhao Y, Zhao C Z, Yang L, Lu Q, Zhang Q, Smith J and Zhao Y 2016 Effects of rapid thermal annealing on the structural, electrical, and optical properties of Zr-doped ZnO thin films grown by atomic layer deposition *Materials* **9** 695
- [25] Yang J, Zhang Y, Qin C, Ding X and Zhang J 2019 Enhanced stability in Zr-doped ZnO TFTs with minor influence on mobility by atomic layer deposition *IEEE Trans. Electron Devices* **66** 1760–5
- [26] Wang F, Lv M, Pang Z, Yang T, Dai Y and Han S 2008 Theoretical study of structural, optical and electrical properties of zirconium-doped zinc oxide *Appl. Surf. Sci.* **254** 6983–6
- [27] Sato H, Minami T and Takata S 1993 Highly transparent and conductive group IV impurity-doped ZnO thin films prepared by radio frequency magnetron sputtering *J. Vac. Sci. Technol. A* **11** 2975–9
- [28] Johnson R W, Hultqvist A and Bent S F 2014 A brief review of atomic layer deposition: from fundamentals to applications *Mater. Today* **17** 236–46
- [29] Mallick B C, Hsieh C-T, Yin K-M, Gandomi Y A and Huang K-T 2019 Review—on atomic layer deposition: current progress and future challenges *ECS J. Solid State Sci. Technol.* **8** N55
- [30] Gao Z and Banerjee P 2019 Review article: atomic layer deposition of doped ZnO films *J. Vac. Sci. Technol. A* **37** 050802
- [31] Poodt P, Knaapen R, Illiberi A, Roozeboom F and van Asten A 2012 Low temperature and roll-to-roll spatial atomic layer deposition for flexible electronics *J. Vac. Sci. Technol. A* **30** 01A142
- [32] Kim H, Wang Z, Hedhili M N, Wehbe N and Alshareef H N 2017 Oxidant-dependent thermoelectric properties of undoped ZnO films by atomic layer deposition *Chem. Mater.* **29** 2794–802
- [33] Pung S-Y, Choy K-L, Hou X and Shan C 2008 Preferential growth of ZnO thin films by the atomic layer deposition technique *Nanotechnology* **19** 435609
- [34] Yuan N Y, Wang S Y, Tan C B, Wang X Q, Chen G G and Ding J N 2013 The influence of deposition temperature on growth mode, optical and mechanical properties of ZnO films prepared by the ALD method *J. Cryst. Growth* **366** 43–6
- [35] Jensen J M, Oelkers A B, Toivola R, Johnson D C, Elam J W and George S M 2002 X-ray reflectivity characterization of ZnO/Al<sub>2</sub>O<sub>3</sub> multilayers prepared by atomic layer deposition *Chem. Mater.* **14** 2276–82
- [36] Geng Y, Xie Z-Y, Yang W, Xu S-S, Sun Q-Q, Ding S-J, Lu H-L and Zhang D W 2013 Structural, optical, and electrical properties of Hf-doped ZnO films deposited by atomic layer deposition *Surf. Coat. Technol.* **232** 41–5
- [37] Holzwarth Ü and Gibson N 2011 The Scherrer equation versus the ‘Debye–Scherrer equation’ *Nat. Nanotechnol.* **6** 534–534
- [38] Zs B et al 2011 Temperature dependent *in situ* doping of ALD ZnO *J. Therm. Anal. Calorim.* **105** 93–9
- [39] Lai C-Y, Santos S, Moser T, Alfakes B, Lu J-Y, Olukan T, Rajput N, Boström T and Chiesa M 2020 Explaining doping in material research (Hf substitution in ZnO films) by directly quantifying the van der Waals force *Phys. Chem. Chem. Phys.* **22** 4130–7
- [40] Ahn C H, Kim J H and Cho H K 2012 Tunable electrical and optical properties in composition controlled Hf:ZnO thin films grown by atomic layer deposition *J. Electrochem. Soc.* **159** H384
- [41] Duan X M, Stampfl C, Bilek M M M, McKenzie D R and Wei S-H 2011 Design of shallow acceptors in ZnO through early transition metals codoped with N acceptors *Phys. Rev. B* **83** 085202
- [42] Ali S, Juntunen T, Sintonen S, Ylivaara O M E, Puurunen R L, Lipsanen H, Tittonen I and Hannula S-P 2016 Thermal conductivity of amorphous Al<sub>2</sub>O<sub>3</sub>/TiO<sub>2</sub> nanolaminates deposited by atomic layer deposition *Nanotechnology* **27** 445704
- [43] Park T-H, Park N-W, Kim J, Lee W-Y, Koh J-H and Lee S-K 2015 Cross-plane temperature-dependent thermal conductivity of Al-doped zinc oxide thin films *J. Alloys Compd.* **638** 83–7
- [44] Alvarez-Quintana J, Martínez E, Pérez-Tijerina E, Pérez-García S A and Rodríguez-Viejo J 2010 Temperature dependent thermal conductivity of polycrystalline ZnO films *J. Appl. Phys.* **107** 063713
- [45] Tynell T, Giri A, Gaskins J, Hopkins P E, Mele P, Miyazaki K and Karppinen M 2014 Efficiently suppressed thermal conductivity in ZnO thin films via periodic introduction of organic layers *J. Mater. Chem. A* **2** 12150–2